Supplement of Atmos. Chem. Phys., 17, 10245–10258, 2017
https://doi.org/10.5194/acp-17-10245-2017-supplement

Supplement of

Impacts of traffic emissions on atmospheric particulate nitrate and organics at a downwind site on the periphery of Guangzhou, China

Yi Ming Qin et al.

Correspondence to: Chak K. Chan (chak.k.chan@cityu.edu.hk) and Yong Jie Li (yongjieli@umac.mo)

Text:

Text S1: $PM_{2.5}$ mass concentration correction

The Grimm monitor was based on particle scattering measurements or called optical particle counter. A $PM_{2.5}$ cut-off was placed before the GRIMM 180. The $PM_{2.5}$ mass concentration by Grimm 180 was corrected by the daily $PM_{2.5}$ mass concentration with quartz filter measurement. We first integrated the hourly Grimm 180 data into daily basis, and then compared with the daily $PM_{2.5}$ mass concentration with quartz filter measurement (PQ200 Ambient Air Particulate Sampler with a $PM_{2.5}$ cut-off). The daily mass concentration by quartz filter sampling was then obtained gravimetrically. The PQ200 and Grimm 180 measurements were in good agreement with R^2 of 0.93, with a slope of PQ200 vs. Grimm 180 data of 1.232 (Figure S3). We then used the linearly fitted parameter to correct the hourly Grimm 180 data to derive the hourly $PM_{2.5}$ mass concentration.

Text S2: Source apportionment for OA

Several source profiles from previously reported HR-ToF-AMS data with different *a* values were explored. However, some ions were missing from the reference source profile when compared with our dataset. For these ions, the signal intensities were estimated based on the unit-mass-resolution (UMR) source profile from the average of multiple ambient data sets (Ng et al., 2011) as follows:

$$I_{\mathrm{m/z}}=k * I_{\mathrm{UMR(m/z)}}-I_{\mathrm{HRrest(m/z)}} \quad (1);$$

$$k= I_{\mathrm{UMR(total)}}/I_{\mathrm{HR(total)}} \quad (2).$$

where $I_{\mathrm{m/z}}$ is the signal intensity of the missing ions in the reference profile; k is a correction factor, derived from the ratio of total signal intensities in the UMR and HR profiles, which accounts for the difference in total signal intensity between the profiles; $I_{\mathrm{UMR(m/z)}}$ is the total signal intensity at UMR level for the missing ions in the UMR profile; and $I_{\mathrm{HRrest(m/z)}}$ is the sum of the signal intensities of the rest of the ions from HR reference profile that shares the same integer m/z as the missing ions. For these ions, whose intensities are derived from the above equation, an *a* value of 1 (100% deviation) was used.

We used the ME-2 solver with reference mass spectra to tackle the problem of mixing sources in our PMF runs. The HOA the Paris campaign (Crippa et al., 2013) as an input reference however were not fitted in our dataset. The resolved-HOA factor contributed no more than 5% of total OA, and only exhibited a small morning rush peak in the diurnal pattern (Fig. S6). Furthermore, another factor was observed to share similar features with the HOA mass spectrum. This factor exhibited clear rush-hour peaks during the morning and late afternoon, as with traffic-related pollutants (e.g. NO_x and BC). Also, the mass fraction of this factor is 3-4 times higher than the resolved-HOA factor. Alternatively, we directly extracted a local HOA source profile (HOA_{loc}) from the data set using a separate PMF run in selected time series with peaks in organic mass concentration. We selected the high OA events in order to capture some periods with potentially high HOA. As shown in Fig S7, the concentrations of other traffic tracers (for example BC and NOx) were also high, indicating the potential influence by high HOA. A similar approach of extracting factors in unconstrained PMF and subsequent combination of duplicate factors was also used in a previous study (Fröhlich et al., 2015). (Fröhlich et al., 2015) Using the peaks or only one peak yield similar mass spectra for local HOA factors with R_{uc}=0.99 (Fig. S7a, S7b). The HOA profiles remained the similar with even more factors (Fig. S7c). We then used the HOA source profile obtained from all of the short peaks as the input HOA source profile (LHOA therein). However, constrained LHOA alone cannot resolved an environmentally reasonable solution either (Fig. S8). We then tried to added other primary OA source profiles as constrain. For COA source profile, we chose the COA source profile from the Hong Kong campaign (HK) to constrain our ME-2 runs as cooking styles and ingredients in Guangzhou are similar to those in Hong Kong. For the BBOA factor, we used the reference BBOA profile from MILAGRO (Aiken et al., 2009). The resolved BBOA factor tracked well with its tracer ion ($C_2H_4O_2^+$) and potassium (K^+) in time series.

A four-factor (HOA, COA, BBOA and a free factor) solution had a higher Q/Q_{exp}, while a six-factor (HOA, COA, BBOA and three free factors) solution seemed to split OOA factors without obvious physical meaning. An five-factor solution with *a* values of 0.1, 0.2, 0.3 for HOA_{local}, COA_{HK}, and $BBOA_{MILAGRO}$, respectively, was finally adopted. The *a* values for these POA factors were also in line with previous ME-2 studies (Canonaco et al., 2013; Crippa et al., 2014; Fröhlich et al., 2015). We further run the ME-2 with the same conditions with 10 runs to explore the stability of solution. The time series and mass spectra for these 10 runs were quite steady (Fig. S10). The final solution came from results obtained with averaging these ten runs. Two oxygenated organic aerosol factors, SVOOA and LVOOA, were assigned based on their degree of oxygenation.

Text S3: Time series and diurnal patterns of meteorological conditions and gas and particle species.

Fig. S11 shows the time series of NR-PM_1 species (sulfate, nitrate, ammonium, chloride, and organics), BC, and meteorological factors (precipitation, RH, temperature, wind direction, and wind speed) for the whole campaign. Northerly winds (hourly integrated) prevailed through the whole campaign. As located at the southerly of downtown Guangzhou, the sampling site was greatly affected by the pollutants transport from downtown area under such condition. NO_x ranged from 9 to 333 ppb, averaging at 40.8 ppb. The high NO_x levels reflect heavy influences from traffic emissions. The high NO_x concentration provided great potential for secondary production of particulate nitrate. Ozone ranged from 0.2 to 119.9 ppb with an average of 22.7 ppb. An episodic high O_3 period occurred from the November 14th to 27th, 2014, and peaked in every afternoon. The average temperature was 5 °C lower in December than in November.

Diurnal patterns for temperature, RH, irradiance (IR), NO_x, O_3, all NR-PM_1 species, and BC in November and December are depicted in Figure S12.

In November, IR, an indicator of photochemical activities, showed a clear noon time peak. Ozone concentration slowly increases after sunrises and reaches its maximum in mid-afternoon. The relatively high IR and O_3 concentrations at noon time indicate the strong photochemical activities. Obvious diurnal cycles of temperature and RH were observed. SO_2 had morning peaks while NO_x showed clear rush hour peaks. Sulfate showed a slight concentration increase in median hourly data in the early morning in November, consistent with the SO_2 morning peaks. The daytime decrease in nitrate and chloride in November may due to the combinative effects of higher mixing layer height and gas-to particle partitioning under high temperature and low RH conditions (Seinfeld and Pandis, 2006). Ammonium concentration decreased in the early morning and increased in late afternoon, which was the combined result of the variations of anions in the particle (sulfate, nitrate and chloride). Organics had a significant increase after 16:00, and stayed at a high level at night, which might be attributed to combined effects of enhanced vehicular emissions and lower mixing layer height. Other vehicle-related pollutants such as NO_x and BC also showed an increase in concentrations after 16:00. Also, a small organics peak appeared in the afternoon, coincided with the peak of O_3, suggesting the possibility of photochemical formation of SOA. The diurnal patterns of individual organic factors as characterized by ME-2 which will be discussed in a later section. Similar diurnal variations for most of the PM_1 species in November were also observed in the earlier field campaign conduced in November in Shenzhen (He et al., 2011).

In December, although O_3 concentrations were significantly lower than those in November, the daytime peak was still obvious. Both temperature and RH were lower in December than in November while obvious diurnal cycles of temperature and RH were also observed. No obvious diurnal variation for SO_2 were observed in December. NO_x still showed clear rush hour peaks. However, a discrepancy between mean and median data in diurnal patterns for NO_x was apparent during night to early morning in December because of intense traffic emissions on 24-25 December, as also shown in the high NO_x concentrations in Figure S11. SO_4 slightly increased at night, which might be attributed to the lower mixing layer height during nighttime. However, nitrate concentration did not experience a significant decrease, while the daytime decrease in chloride is still obvious. Other contributing factors of nitrate may somewhat offset the decrease due to higher mixing layer height and evaporation from particles in daytime. Ammonium concentration increased in late afternoon, which was the combined result of the variations of anions in the particle. Organics had a significant increase after 16:00, stayed at a high level at night, and tracked well with vehicle-related pollutants such as NO_x and BC.

Text S4: Organic nitrate and inorganic nitrate estimation

To exanimate the interference of organic nitrate (ON) to our analysis in the nitrate formation, we adopted two methods to estimate the ON concentration. The first method (Method 1, therein) is using the ratio of NO^+/NO_2^+(Farmer et al., 2010), which takes the advantage of the difference of NO^+/NO_2^+ in organic nitrate and ammonium nitrate. The fraction of the total nitrate signal due to organic nitrate(x) can be derived from:

$$x = \frac{(R_{obs} - R_{NH4NO3})(1 + R_{ON})}{(R_{ON} - R_{NH4NO3})(1 + R_{obs})} \quad (1)$$

where R_{obs} is the NO^+/NO_2^+in the ambient observation, R_{NH4NO3} is the NO^+/NO_2^+ of ammonium nitrate in IE calibration, while R_{ON} is the NO^+/NO_2^+ of ON. Xu et al.(2015) suggested that the NO^+/NO_2^+ values of 5 and 10 likely correspond to the upper and lower bounds of the ratios from ON. Such a boundary using NO^+/NO_2^+ method is adopted in this study for the estimation of organic nitrate's contribution to the AMS nitrate concentration. The organic nitrate can be derived by multiplying the organic nitrate fraction (x) with the total nitrate in AMS. And the inorganic nitrate can then be calculated by subtracting the organic nitrate from the total nitrate concentration. But still, we should be cautious in this method as the vast array of possible ON parent compounds in ambient particles and the in consistency of the ratio between instruments may led to some bias in the calculation. We also use the organic concentration and elemental ratio (OM:OC and N:C) from HR-ToF-AMS measurement to estimate the lower bounder of organic nitrate (Method 2, therein) adopted from Schurman et al.(2015).

ON_{min}=(Organics/OM:OC)*N: C*(14/12) (2)

where Organics is total organic concentration. ON may be underestimated using this method as N:C includes only N from CHON and CHN fragments. The maximum inorganic nitrate can also be estimated by deducting the ON_{min} from the total nitrate concentration in this method.

The time series of total nitrate form AMS and MAGRA, and inorganic nitrate and organic nitrate calculated from Method 1 and Method 2 are shown in Fig. S13, while the campaign average mass concentration and mass fraction derived from each method are shown in Fig. S14-S15. On average, the maximum IN concentration estimated from Method 1 was 6.15 μg/m^3, accounted for 81.2% of the total nitrate mass concentration from AMS measurement. And the minimum IN concentration from Method 1 was 4.95 μg/m^3, contributed to 74.4% of the total nitrate mass. While using Method 2, the minimum nitrate was 6.48 μg/m^3, accounted for 89.8 % of the total nitrate. And the time series of the calculated inorganic was tracked well with the total AMS measured nitrate (Fig. S13). Fig. 2 shows the scatter plot of estimated inorganic nitrate versa total AMS measured nitrate. We found that the estimated inorganic nitrate was highly correlated with ($R_p^2 \geq 0.95$) with the total AMS nitrate concentration and followed with the 1 to 1 line for each method we used. Even though organic nitrate also contributed to the total nitrate we measured, both the variation and the concentration of the nitrate did not change a lot after subtracting the organic nitrate. Furthermore, as shown in Fig. S2, AMS measured nitrate were comparable to those from MAGRA, with a correlation slope of 0.9 and a R_p of 0.95. Given the uncertainties associated with each estimations, we conservatively used the total HR-ToF-AMS nitrate concentration in our discussion.

Figures and Tables:

Figure S 1 Location of sampling site

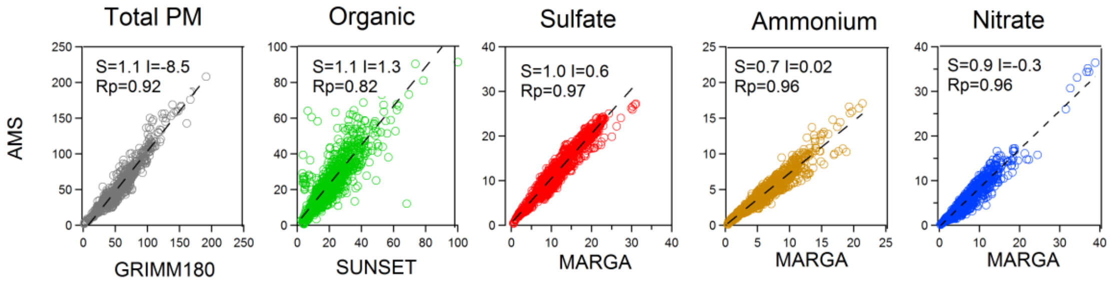

Figure S 2 AMS data comparison

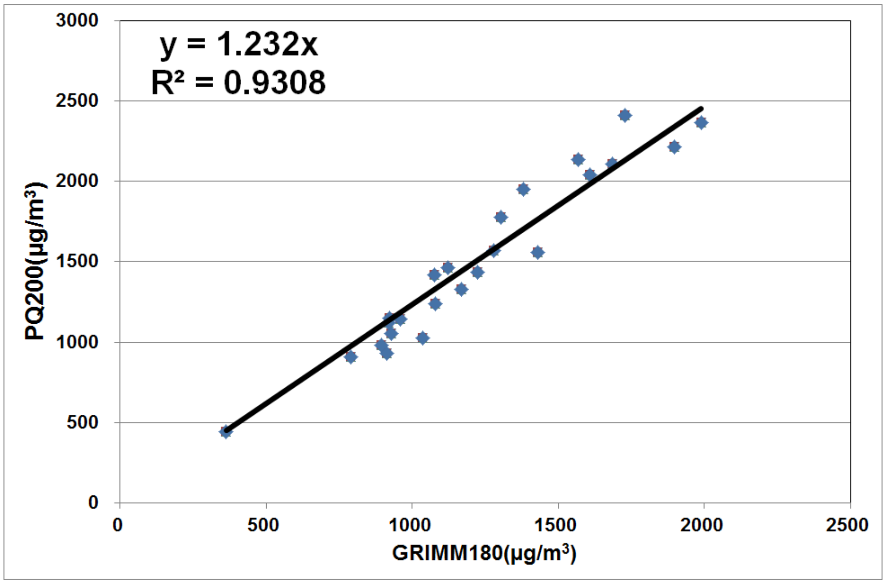

Figure S 3 PM2.5 comparison between PQ200 and GRIMM180

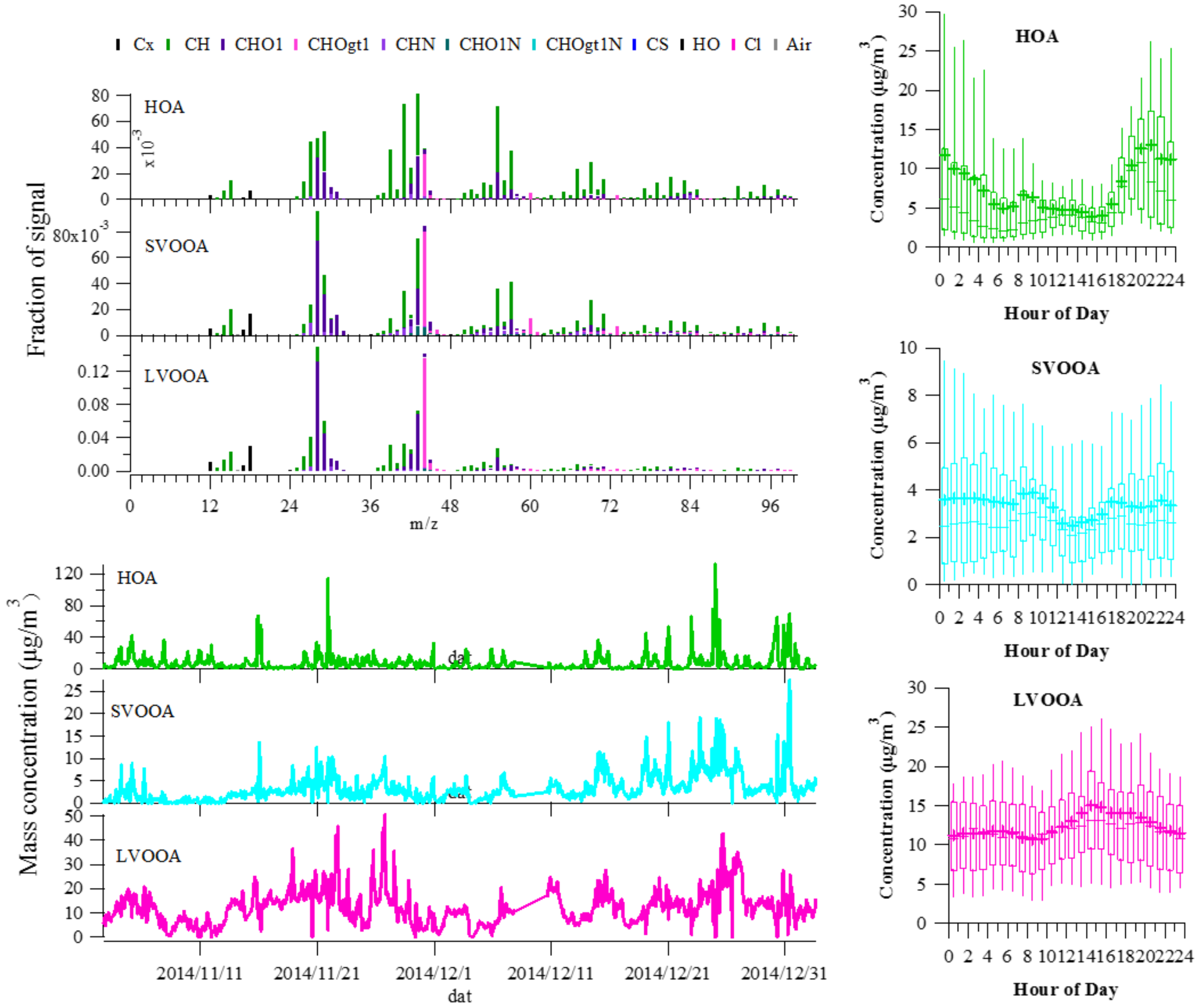

Figure S 4 Three factors PMF solution

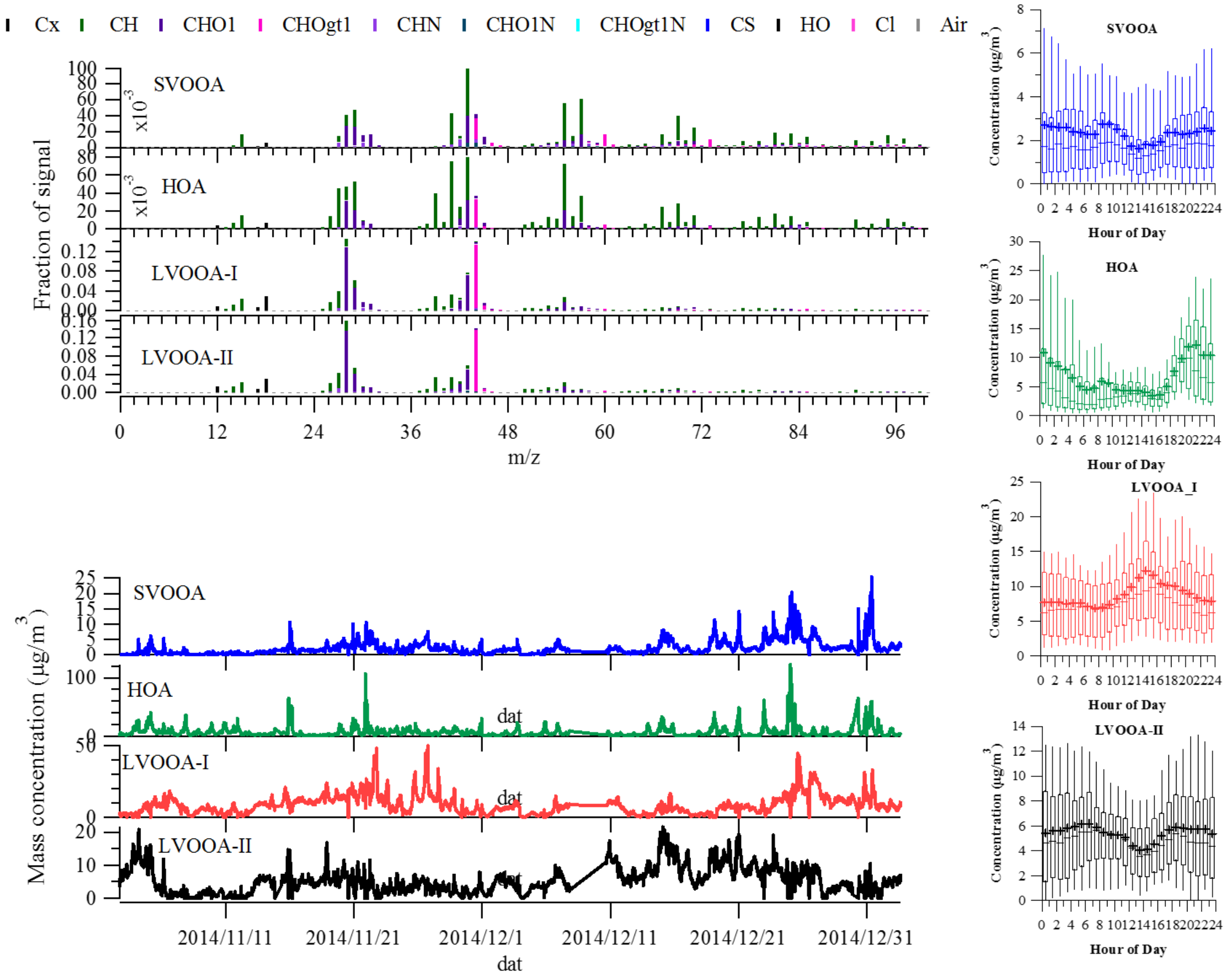

Figure S 5 Four factors PMF solution

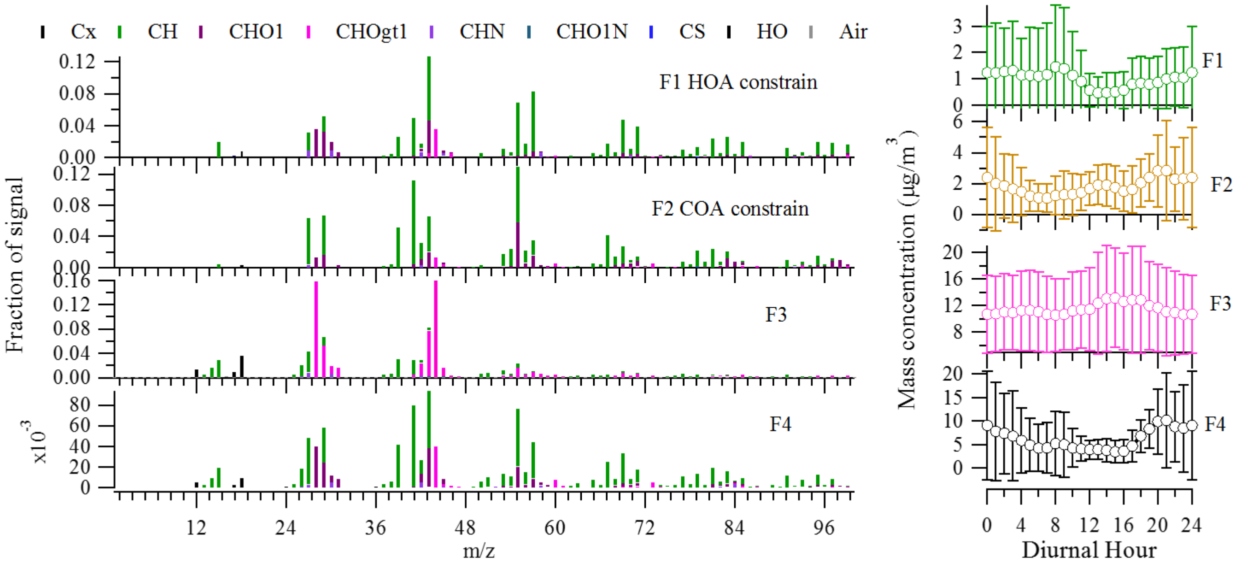

Figure S 6 Factor profiles and diurnal variations in ME-2 trials. four factor solution with constraining HOA and COA, which are adopted from Paris Campaign(Crippa et al., 2013).

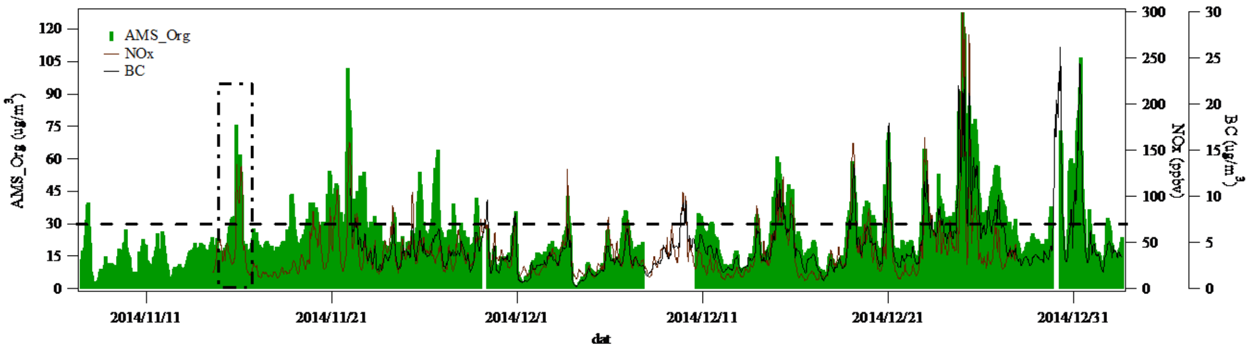

Figure S 7 Organic peaks during the campaign

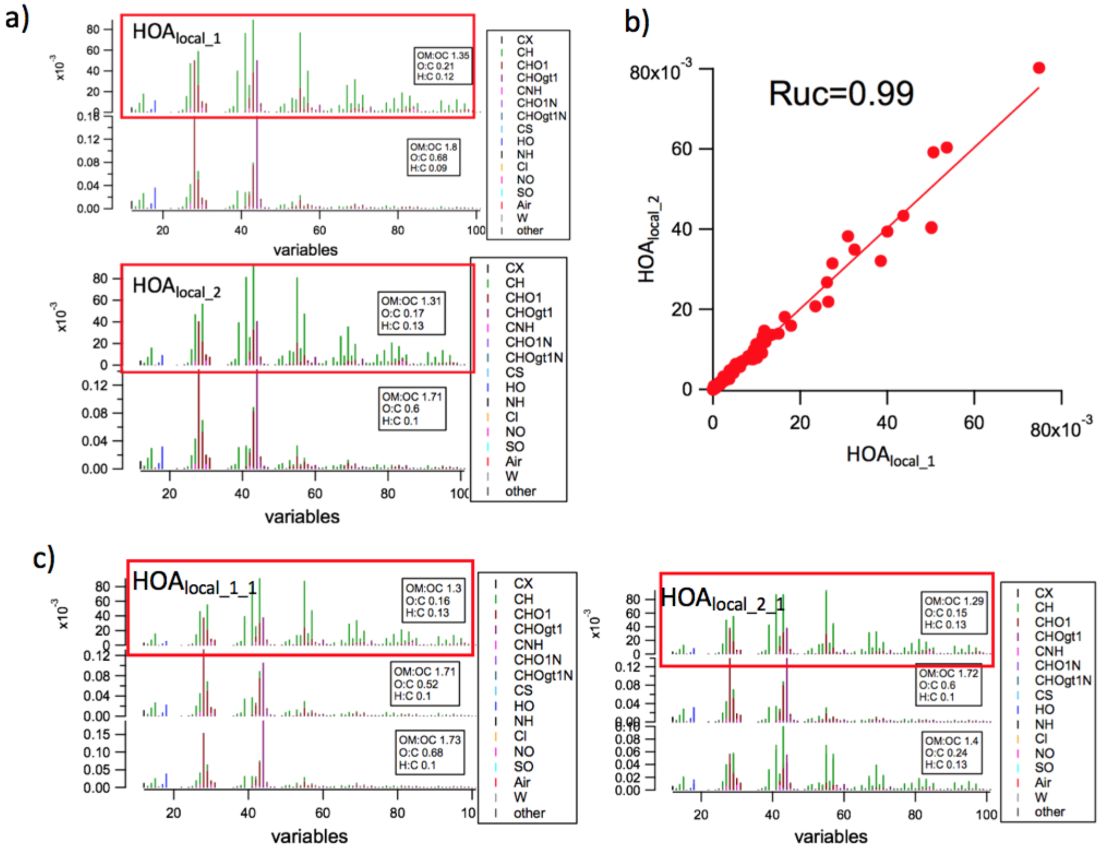

Figure S 8 Local HOA source profile comparison

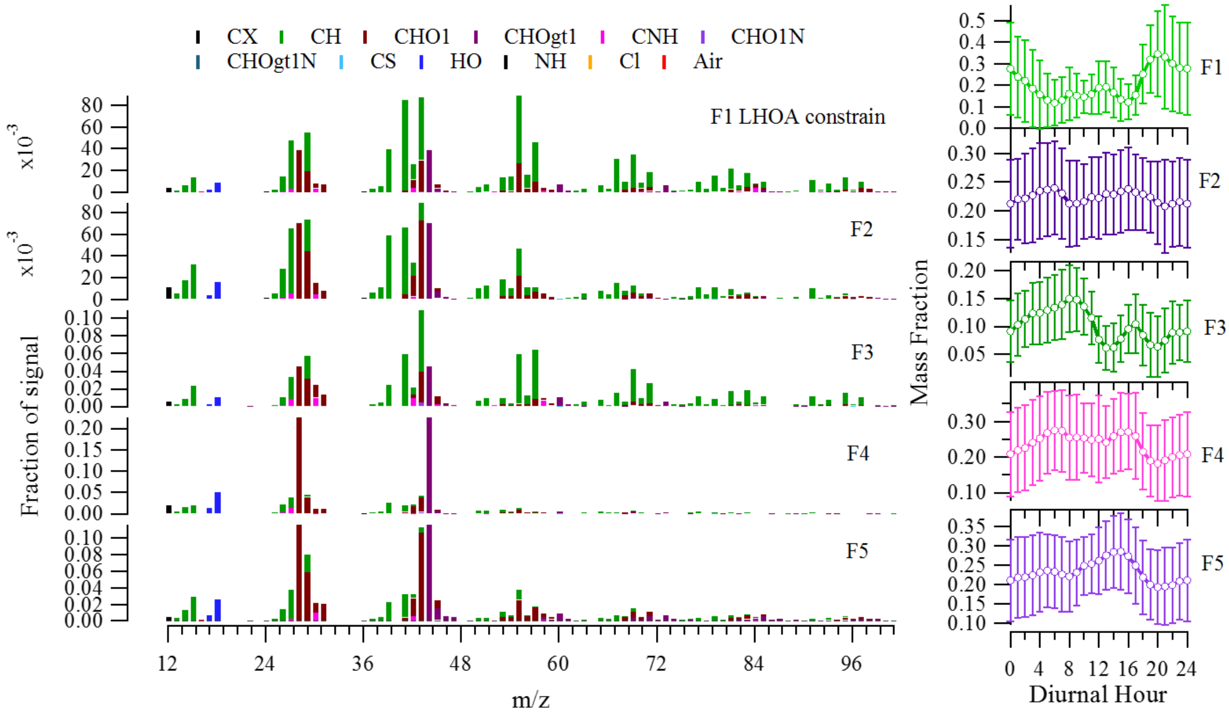

Figure S 9 Five factor solution with LHOA constrain

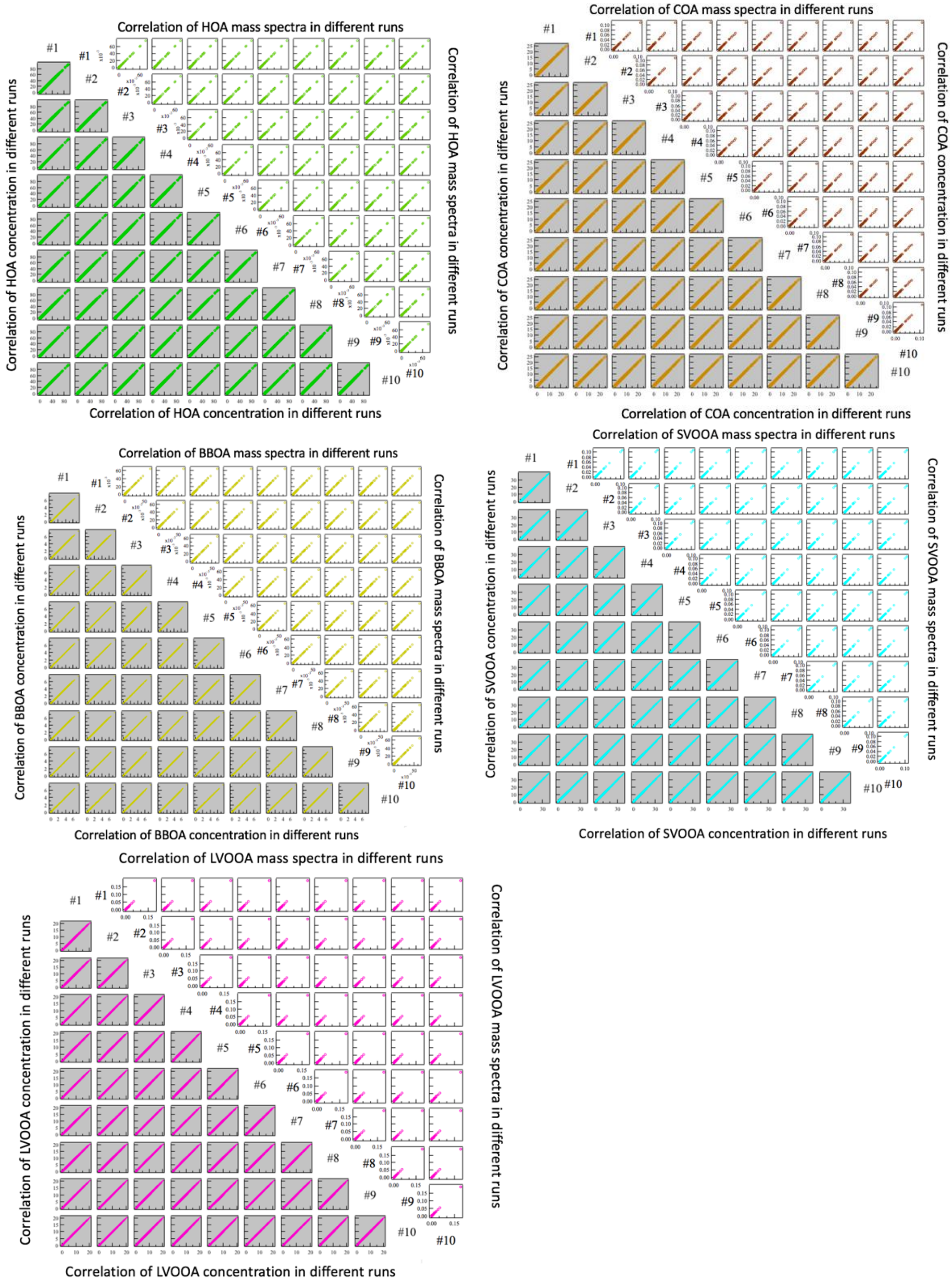

Figure S 10 Correlation of the time series and mass spectra for ten runs with optimal solution.

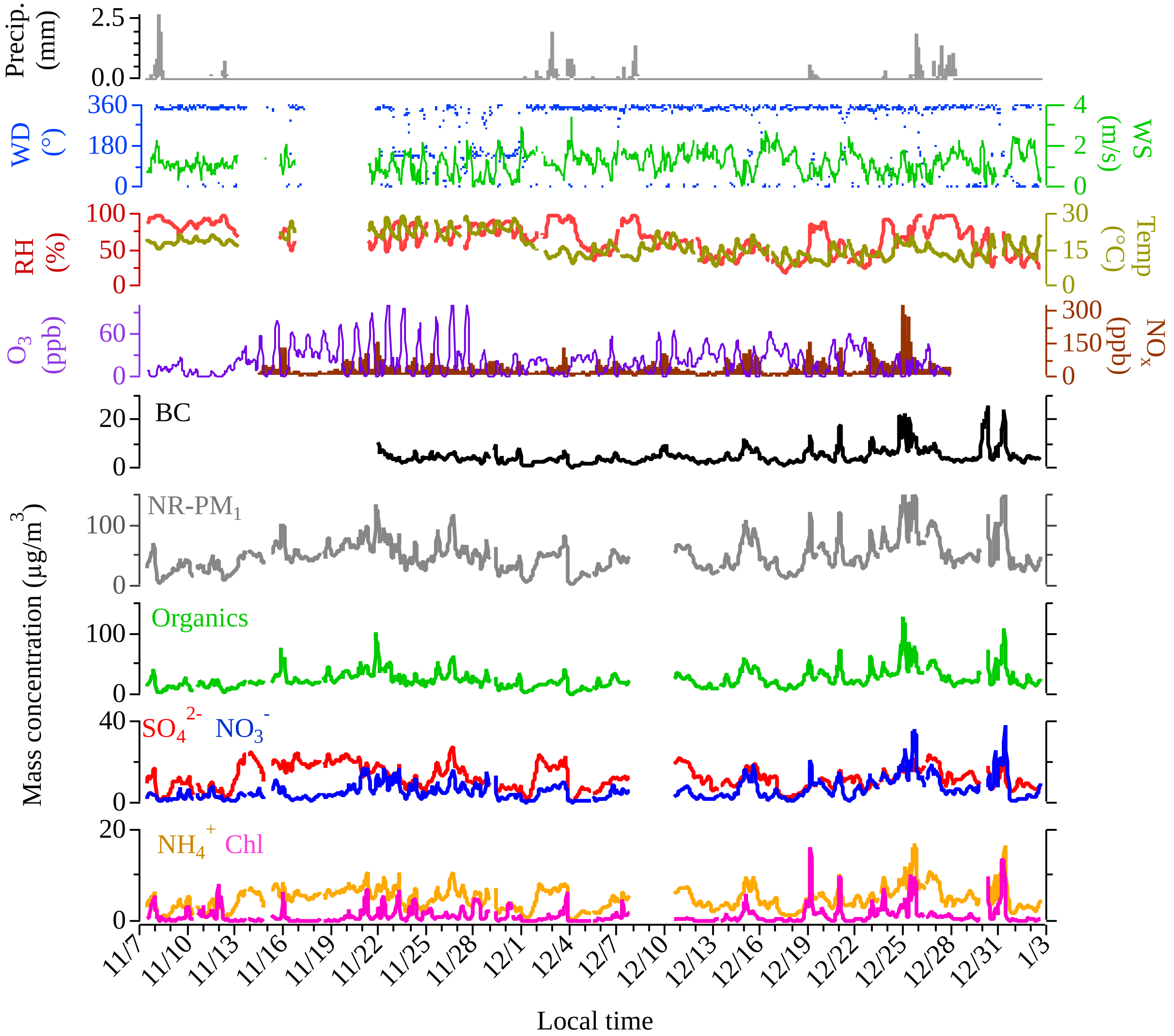

185

186 *Figure S 11 Time series of NR-PM₁ species (sulfate, nitrate, ammonium, chloride, and organics), BC, and meteorological factors*

187 *(precipitation, relative humidity, temperature, wind direction and wind speed) for the campaign. Hourly averages are shown.*

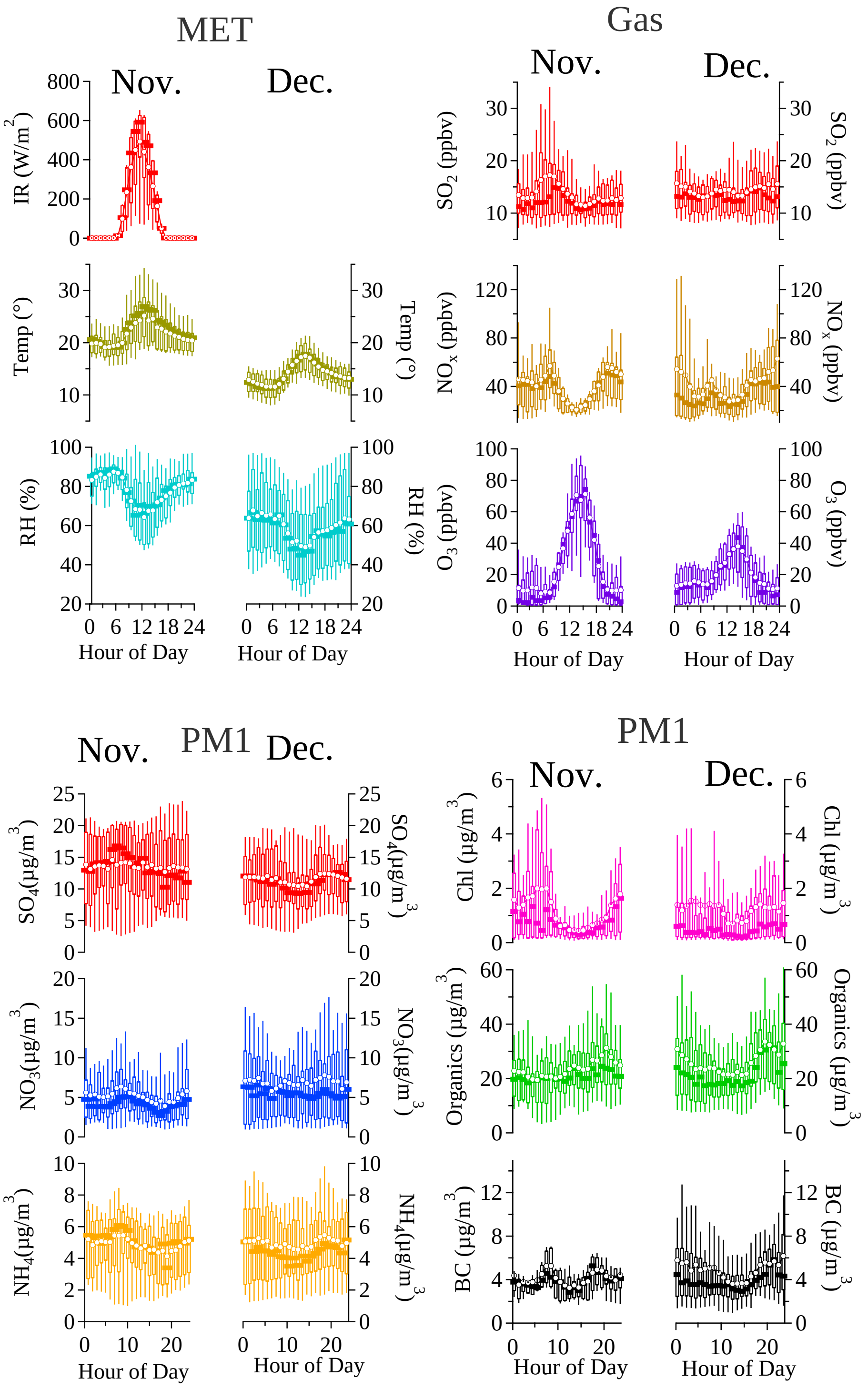

Figure S 12 Diurnal patterns for temperature, RH, Irradiance, NO_x, O_3, all NR-PM_1 species, and BC in Nov. and Dec. (25th and 75th percentile boxes,5th and 95th percentile whiskers, median as line in solid dot, and mean as cycle). There is no Irradiance data available in December

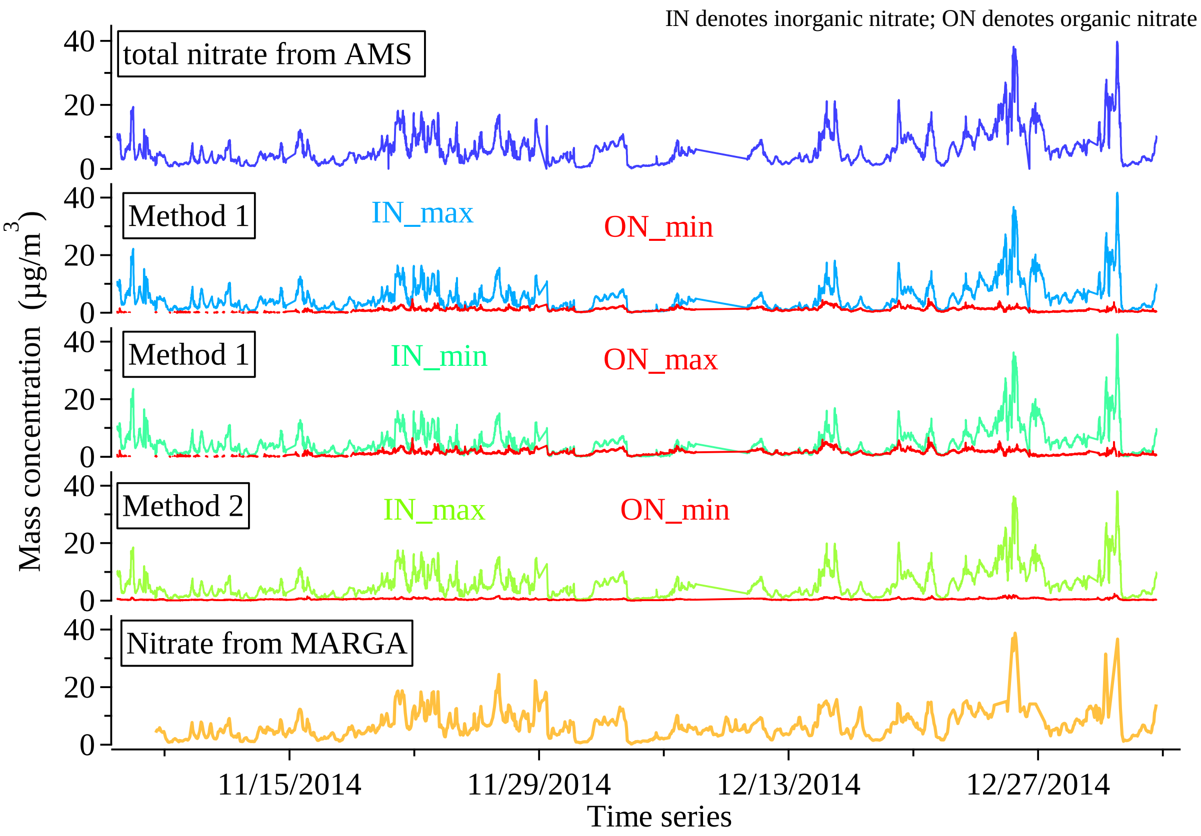

Figure S 13 Time series of total nitrate form AMS and MAGRA and , inorganic nitrate and organic nitrate calculated from Method 1 and Method 2. IN denotes inorganic nitrate and ON denotes organic nitrate.

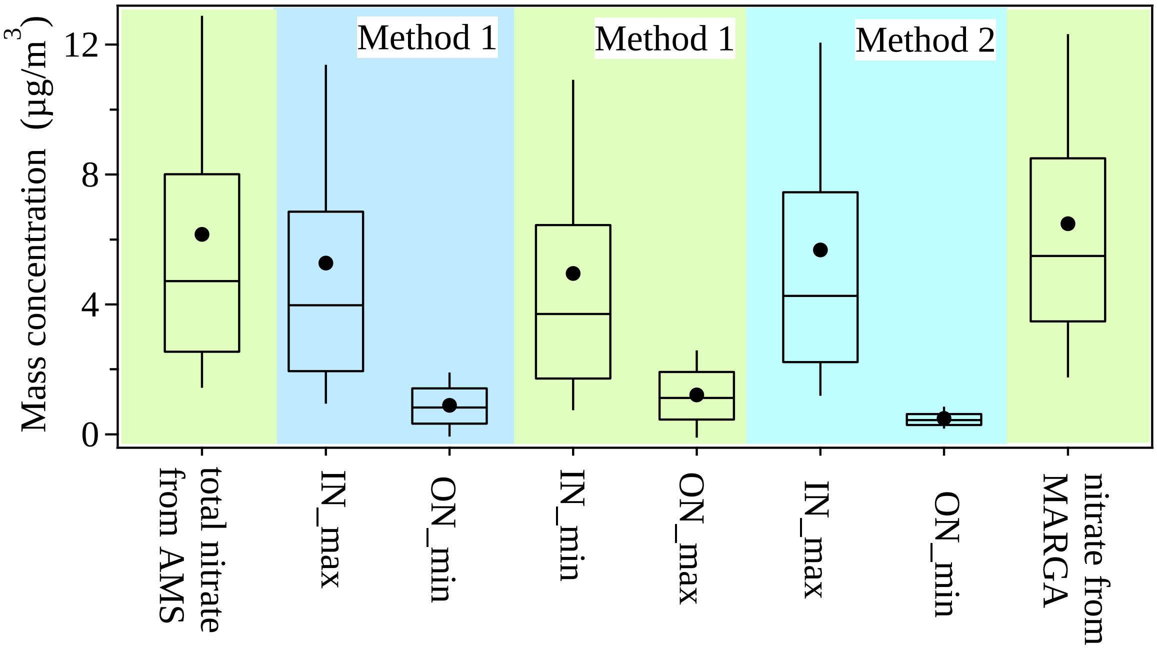

Figure S 14 Box and whisker plot of nitrate mass concentration from AMS and MAGRA, and inorganic nitrate and organic nitrate calculated from Method 1 and Method 2 (25th and 75th percentile boxes, 10th and 90th percentile whiskers, median as line in solid line, and mean as dot).

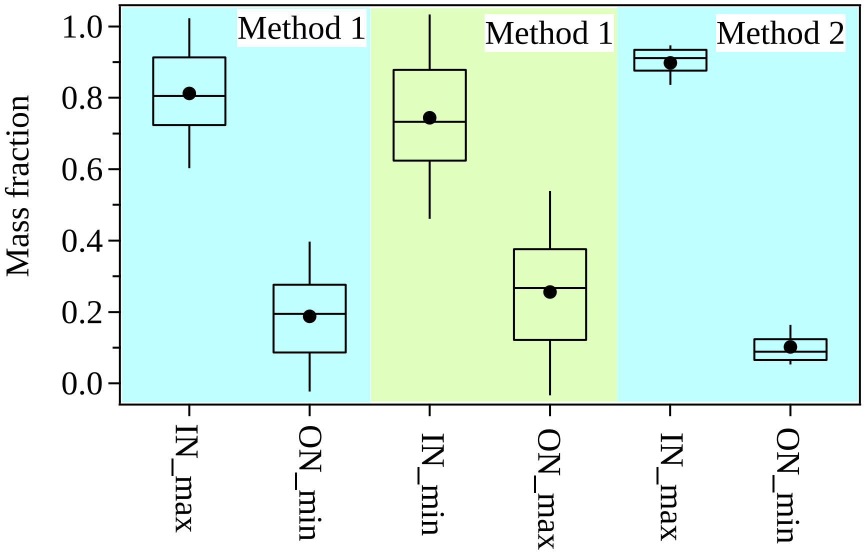

Figure S 15 Box and whisker plot of inorganic nitrate and organic nitrate mass fraction calculated from Method 1 and Method 2 (25th and 75th percentile boxes, 10th and 90th percentile whiskers, median as line in solid line, and mean as dot).

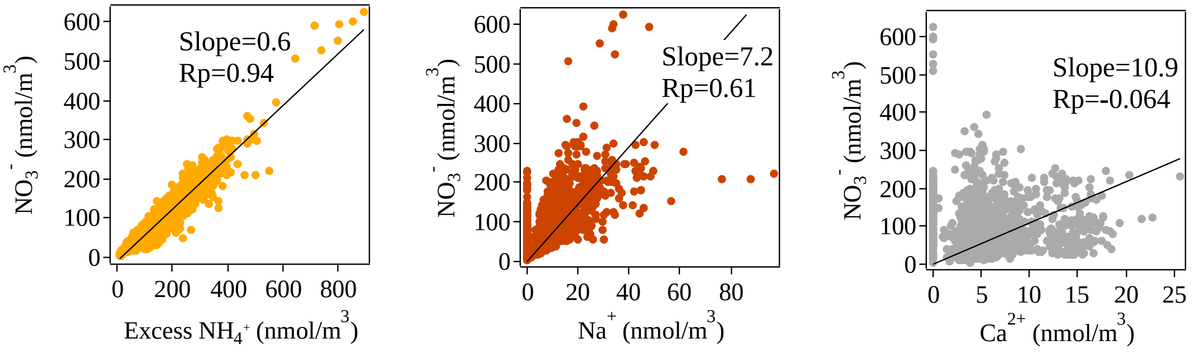

Figure S 16. Scatter plots of NO3-molar concentration from MARGA (PM2.5) against those of excess NH4+, Na+ and Ca2+.

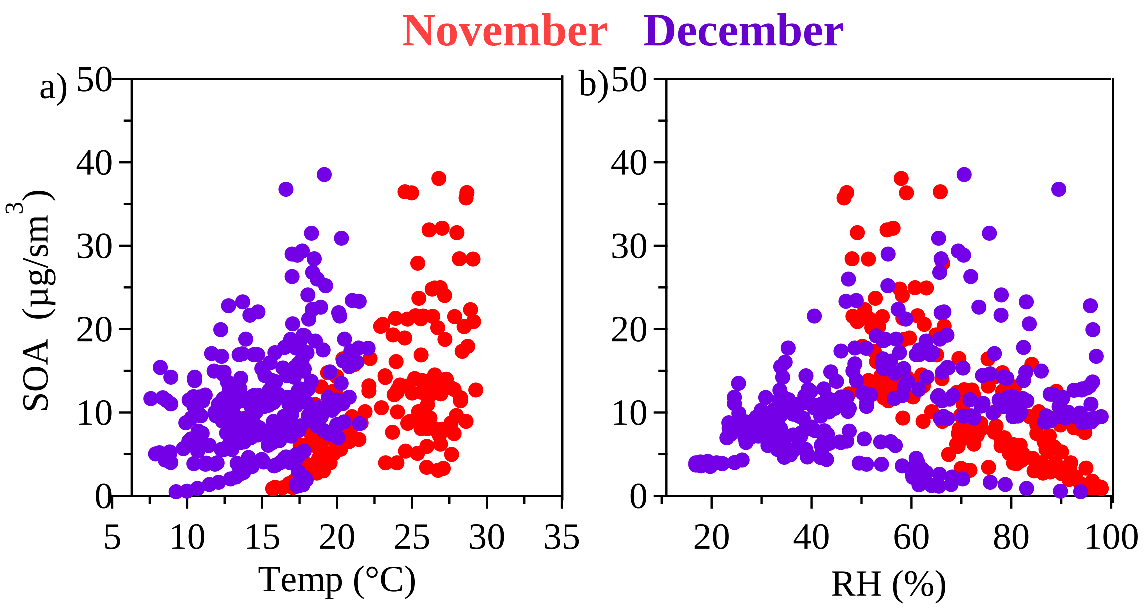

Figure S 17. (a)SOA against temperature; (b) SOA against LWC during the day.

Table S 1 Correlation of ME-2 resolved OA factors with tracers

Correlation (R_p)	NO_x	C_3H_3O	$C_2H_4O_2$	NO_3	SO_4
HOA	0.83	0.84	0.81	0.58	0.18
COA	0.51	0.66	0.42	0.08	0.08
BBOA	0.18	0.47	0.71	0.52	0.33
LVOOA	-0.01	0.31	0.42	0.43	0.7
SVOOA	0.21	0.66	0.62	0.68	0.49

References:

Aiken, A. C., Salcedo, D., Cubison, M. J., Huffman, J. A., DeCarlo, P. F., Ulbrich, I. M., Docherty, K. S., Sueper, D., Kimmel, J. R., Worsnop, D. R., Trimborn, A., Northway, M., Stone, E. A., Schauer, J. J., Volkamer, R. M., Fortner, E., de Foy, B., Wang, J., Laskin, A., Shutthanandan, V., Zheng, J., Zhang, R., Gaffney, J., Marley, N. A., Paredes-Miranda, G., Arnott, W. P., Molina, L. T., Sosa, G. and Jimenez, J. L.: Mexico City aerosol analysis during MILAGRO using high resolution aerosol mass spectrometry at the urban supersite (T0) – Part 1: Fine particle composition and organic source apportionment, Atmos. Chem. Phys., 9(17), 6633–6653, doi:10.5194/acp-9-6633-2009, 2009.

Canonaco, F., Crippa, M., Slowik, J. G., Baltensperger, U. and Prévôt, A. S. H.: SoFi, an IGOR-based interface for the efficient use of the generalized multilinear engine (ME-2) for the source apportionment: ME-2 application to aerosol mass spectrometer data, Atmos. Meas. Tech., 6(12), 3649–3661, doi:10.5194/amt-6-3649-2013, 2013.

Crippa, M., El Haddad, I., Slowik, J. G., DeCarlo, P. F., Mohr, C., Heringa, M. F., Chirico, R., Marchand, N., Sciare, J., Baltensperger, U. and Prévôt, A. S. H.: Identification of marine and continental aerosol sources in Paris using high resolution aerosol mass spectrometry, J. Geophys. Res. Atmos., 118(4), 1950–1963, doi:10.1002/jgrd.50151, 2013.

Crippa, M., Canonaco, F., Lanz, V. A., Äijälä, M., Allan, J. D., Carbone, S., Capes, G., Ceburnis, D., Dall’Osto, M., Day, D. A., DeCarlo, P. F., Ehn, M., Eriksson, A., Freney, E., Hildebrandt Ruiz, L., Hillamo, R., Jimenez, J. L., Junninen, H., Kiendler-Scharr, A., Kortelainen, A.-M., Kulmala, M., Laaksonen, A., Mensah, A. A., Mohr, C., Nemitz, E., O’Dowd, C., Ovadnevaite, J., Pandis, S. N., Petäjä, T., Poulain, L., Saarikoski, S., Sellegri, K., Swietlicki, E., Tiitta, P., Worsnop, D. R., Baltensperger, U. and Prévôt, A. S. H.: Organic aerosol components derived from 25 AMS data sets across Europe using a consistent ME-2 based source apportionment approach, Atmos. Chem. Phys., 14(12), 6159–6176, doi:10.5194/acp-14-6159-2014, 2014.

Farmer, D. K., Matsunaga, a, Docherty, K. S., Surratt, J. D., Seinfeld, J. H., Ziemann, P. J. and Jimenez, J. L.: Response of an aerosol mass spectrometer to organonitrates and organosulfates and implications for atmospheric chemistry., Proc. Natl. Acad. Sci. U. S. A., 107(15), 6670–6675, doi:10.1073/pnas.0912340107, 2010.

Fröhlich, R., Crenn, V., Setyan, A., Belis, C. A., Canonaco, F., Favez, O., Riffault, V., Slowik, J.

G., Aas, W., Aijälä, M., Alastuey, A., Artiñano, B., Bonnaire, N., Bozzetti, C., Bressi, M., Carbone, C., Coz, E., Croteau, P. L., Cubison, M. J., Esser-Gietl, J. K., Green, D. C., Gros, V., Heikkinen, L., Herrmann, H., Jayne, J. T., Lunder, C. R., Minguillón, M. C., Močnik, G., O'Dowd, C. D., Ovadnevaite, J., Petralia, E., Poulain, L., Priestman, M., Ripoll, A., Sarda-Estève, R., Wiedensohler, A., Baltensperger, U., Sciare, J. and Prévôt, A. S. H.: ACTRIS ACSM intercomparison – Part 2: Intercomparison of ME-2 organic source apportionment results from 15 individual, co-located aerosol mass spectrometers, Atmos. Meas. Tech., 8(6), 2555–2576, doi:10.5194/amt-8-2555-2015, 2015.

He, L.-Y., Huang, X.-F., Xue, L., Hu, M., Lin, Y., Zheng, J., Zhang, R. and Zhang, Y.-H.: Submicron aerosol analysis and organic source apportionment in an urban atmosphere in Pearl River Delta of China using high-resolution aerosol mass spectrometry, J. Geophys. Res., 116(D12), D12304, doi:10.1029/2010JD014566, 2011.

Ng, N. L., Canagaratna, M. R., Jimenez, J. L., Zhang, Q., Ulbrich, I. M. and Worsnop, D. R.: Real-time methods for estimating organic component mass concentrations from aerosol mass spectrometer data, Environ. Sci. Technol., 45(3), 910–916, doi:10.1021/es102951k, 2011.

Schurman, M. I., Lee, T., Desyaterik, Y., Schichtel, B. A., Kreidenweis, S. M. and Collett, J. L.: Transport, biomass burning, and in-situ formation contribute to fine particle concentrations at a remote site near Grand Teton National Park, Atmos. Environ., 112, 257–268, doi:10.1016/j.atmosenv.2015.04.043, 2015.

Seinfeld, J. H. and Pandis, S. N.: ATMOSPHERIC From Air Pollution to Climate Change SECOND EDITION., 2006.

Xu, L., Suresh, S., Guo, H., Weber, R. J. and Ng, N. L.: Aerosol characterization over the southeastern United States using high-resolution aerosol mass spectrometry: spatial and seasonal variation of aerosol composition and sources with a focus on organic nitrates, Atmos. Chem. Phys., 15(13), 7307–7336, doi:10.5194/acp-15-7307-2015, 2015.